Performance Analysis of Intelligent Reflecting Surface-Assisted Orbital Angular Momentum-Based Communication Systems

Kosei Ono, Kazutoshi Yoshii, Megumi Saito, Zhenni Pan, Jiang Liu, Shigeru Shimamoto

Department of Communications and Computer Engineering, School of Fundamental Science and Engineering,
Waseda University, 8-01A, 66 Bldg., 3-14-1 Ohkubo, Shinjuku-ku, Tokyo, Japan

{seikou696@asagi., kazutoshi@suou., megumi.saitou@ruri., zhenni.pan@aoni., jiang@, shima@}waseda.jp

Abstract— **Uniformed circular array antenna (UCA) based orbital angular momentum (OAM) communication system has some disadvantages, such as not being suitable for long-distance multiplexing and requiring a high degree of synchronization between the transmitting and receiving antennas. To achieve non-line-of-sight (NLoS) communication using OAM radio waves, we propose an inter-mode interference (IMI) cancellation method for intelligent reflecting surface (IRS)-Assisted OAM multiplexing to eliminate the IMI from all OAM modes. We also propose a L2-ball projection method to optimize the transmit power allocation for OAM modes to increase the system capacity of IRS-assisted OAM communication systems. The IMI cancellation method and the L2-ball projection method are shown to achieve increasing the maximum system capacity as compared to the L1-ball projection method when the IRS is located closer to the middle between the transmitter UCA and receiver UCA.**

Keywords—**orbital angular momentum (OAM), spatial multiplexing, unified circular array antenna (UCA), intelligent reflecting surface (IRS), inter-mode interference (IMI) cancellation**

I. Introduction

In a wireless communication system, it is important to make effective use of the bandwidth available because of the restricted frequency resource [1]. With the rapid spread of mobile phones since the 1990s, the idea of multiplexing has been developed to enable more people to send and receive data more efficiently at the same time in order to cope with the ever-increasing communication traffic. A recent spread of smartphones and other wireless devices has further increased data traffic in communication networks. In order to respond to the demand for high-speed, large-capacity, and multi-device connections, the orbital angular momentum (OAM) mode multiplexing in a line-of-sight (LoS) environment is attracting attention [2] since it can generate an unlimited number of orthogonal beams not only in circularly symmetric waveguides but also in free space.

Several approaches have been proposed to generate OAM radio waves in real space, using spiral phase plates [3] and UCAs [4]. Uniformed circular array antenna (UCA) is a group of antennas in which the antenna elements are arranged in a circular pattern, and it is possible to generate radio waves with OAM characteristics by shifting the timing of the radiation from the antenna elements. However, the UCA-based OAM communication system has some disadvantages, such as not being suitable for long-distance multiplexing and requiring a high degree of synchronization between the transmitting and receiving antennas. First, the receiving antenna needs to be placed in the same plane as the transmitting antenna. The beam axis misalignment between the transmitter and receiver antennas causes inter-mode interference (IMI), which results in a loss of orthogonality between modes. These physical limitations make long-range multiplexing and reception of OAM radio waves difficult. Secondly, OAM radio waves tend to diverge in the air as the flight distance increases [5].

Several IMI suppression methods in OAM multiplexing have been proposed [6], and [7]. In [6], the IMI is directly eliminated after the discrete Fourier transform (DFT) processing. Conversely, in [7], IMI is suppressed before the DFT processing using the misalignment detection obtained from the angle of arrival estimation.

Current OAM-related works focus on the LoS scenarios, but there are always exist fading or blockages in many practical scenarios. To break the bottleneck of the non-LoS (NLoS) communication, NLoS OAM-MIMO communication systems are analyzed in [8], [9].

Intelligent reflecting surface (IRS) is proposed to achieve NLoS OAM communication [10]. IRS is a reflector that can reflect a signal by adjusting its amplitude and phase by utilizing many low-cost reflecting passive elements [11]. By densely deploying IRSs in a wireless network and smartly coordinating their reflections, it is possible to deliver radio waves to NLoS users and to improve the power strength of edge users by relaying them [12].

In this paper, we propose an IMI cancellation method for IRS-assisted OAM multiplexing to eliminate the IMI from all OAM modes, which can reduce the computational load of equalization. We also propose a ℓ_2-ball (L2-ball) projection method to optimize the transmit power allocation for OAM modes to increase the capacity of IRS-assisted OAM communication systems. The IMI cancellation method and the ℓ_2-ball projection method are shown to achieve increasing the maximum system capacity as compared to the ℓ_1 -ball projection method when the IRS is located closer to the middle between the transmitter UCA and receiver UCA.

II. WIRELESS OAM-BASED COMMUNICATION MODEL

A. System model of an IRS-assisted OAM communication system.

In this section, we introduce an IRS-assisted OAM communication system. We denote the transmitter UCA and receiver UCA by U_T and U_R, respectively, in this paper. Fig. 1 assumes that the center of U_T and the center of U_R are on the z-axis, and the IRS is located in the yz plane, where N_T and N_R denote the number of elements of U_T and U_R, respectively. The radii of U_T and U_R are R_T and R_R, respectively. The number of elements of U_T and U_R are N_T and N_R, respectively. D, $x_{I,O}$, and $z_{I,O}$ denote the distance between U_T and U_R, the distance between U_T and the IRS along the x-axis, and the distance between U_T and the IRS along the z-axis, respectively. Every antenna element of U_T and U_R is arranged equidistantly around a ring, so the phase difference of adjacent elements is $2\pi l / N_i$, where $i \in \{T, R\}$, $-min\{NT, NR\}/2 < l < min\{NT, NR\}/2$ denotes mode index [13][14]. The OAM mode group can be denoted as $\mathcal{L} = \{0, \cdots, L-1\}$, where L denotes the number of multiplexed OAM modes. In this system, we assume that there is no direct link between U_T and U_R due to some obstacles' blocking, so an IRS is applied to establish an alternative LoS route between them.

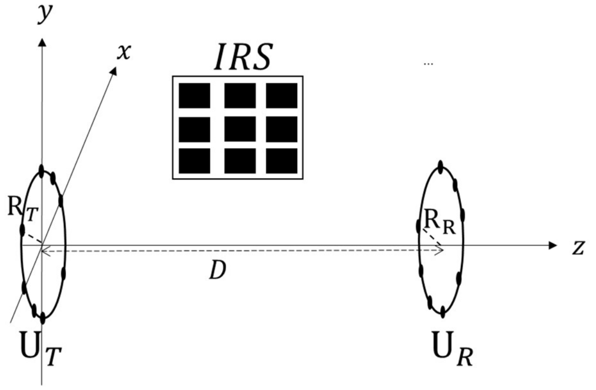

(a) Three-dimensional model.

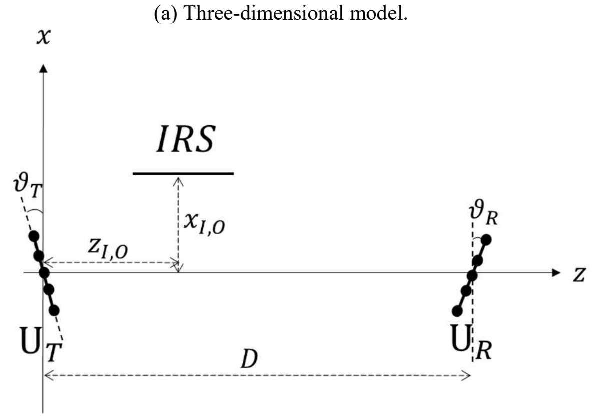

(b) Projection on the xz plane

Figure 1. The geometrical model of the IRS assisted UCA-based OAM system.

We consider the coordinates of U_T, U_R, and each element of the IRS in three-dimensional space [10]. The center points of U_T, U_R, and the IRS is expressed by $\boldsymbol{\omega}_{T,O} = [0,0,0]^T$, $\boldsymbol{\omega}_{R,O} = [0,0,D]^T$, and $\boldsymbol{\omega}_{I,O} = [x_{I,O}, 0, z_{I,O}]^T$, respectively. The coordinate of the n_T-th ($n_T = 1, 2, \cdots, N_T$) antenna element on U_T is

$$\boldsymbol{\omega}_{T,n_T} = \boldsymbol{Q}_y(\vartheta_T) R_T \left[\cos(\varphi_{T,n_T}), \sin(\varphi_{T,n_T}), 0\right]^T \quad (1)$$

where $\varphi_{T,n_T} = \frac{2\pi n_T}{N_T} + \varphi_0$ and $\vartheta_T = \arctan\left(\frac{x_{I,O}}{z_{I,O}}\right)$ denote the phase of the n_T-th elements and the angle of U_T 's rotation around the y-axis. Similarly, the coordinate of the n_R-th ($n_R = 1, 2, \cdots, N_R$) antenna element on U_R can be given by

$$\boldsymbol{\omega}_{R,n_R} = \boldsymbol{Q}_y(\vartheta_R) R_R \left[\cos(\varphi_{R,n_R}), \sin(\varphi_{R,n_R}), 0\right]^T \quad (2)$$

where $\varphi_{R,n_R} = \frac{2\pi n_R}{N_R} + \varphi_0$, $\vartheta_R = \arctan\left(\frac{x_{I,O}}{D - z_{I,O}}\right)$ denotes the phase of the n_R-th elements and the angle of U_R's rotation around the y-axis. The rotation matrix $\boldsymbol{Q}_y(\vartheta_T)$ around the y-axis in (1) and (2) can be given by

$$\boldsymbol{Q}_y(\vartheta) = \begin{bmatrix} \cos\vartheta & 0 & \sin\vartheta \\ 0 & 1 & 0 \\ -\sin\vartheta & 0 & \cos\vartheta \end{bmatrix} \quad (3)$$

where ϑ represents the rotation angle. The coordinates of all the antenna elements on U_T and U_R are $\boldsymbol{\Omega}_T = [\boldsymbol{\omega}_{T,1}, \ldots, \boldsymbol{\omega}_{T,N_T}] \in \mathbb{R}^{3\times N_T}$ and $\boldsymbol{\Omega}_R = [\boldsymbol{\omega}_{R,1}, \ldots, \boldsymbol{\omega}_{R,N_T}] \in \mathbb{R}^{3\times N_R}$, respectively.

c

$$\begin{aligned} &\Omega_I \\ &= \boldsymbol{\omega}_{I,O}\, \mathbf{1}_M^T + \left[\mathbf{0}_M, \left(\boldsymbol{m}_y \mathbf{1}_{M_z} + \frac{1-M_y}{2}\right) d_y, \left(\boldsymbol{m}_y \mathbf{1}_{M_z} + \frac{1-M_y}{2}\right) d_z\right]^T \\ &= \begin{bmatrix} x_{I,O} \cdots\cdots x_{I,O} \\ 0 \cdots\cdots 0 \\ z_{I,O} \cdots\cdots z_{I,O} \end{bmatrix} \\ &+ \begin{bmatrix} 0\cdots & 0 & 0\cdots & 0 & \cdots & 0 & \cdots & 0 \\ 0\cdots & 0 & d_y\cdots & d_y & \cdots(M_y-1)d_y & \cdots & (M_y-1)d_y \\ 0\cdots(M_z-1)d_z & 0 & \cdots(M_z-1)d_z\cdots & & 0 & & \cdots(M_z-1)d_z \end{bmatrix} \quad (4) \end{aligned}$$

where d_y and d_z denote the element separation distances along the y-axis and z-axis of the IRS, respectively. $\boldsymbol{m}_y = [0, \ldots, M_y - 1]^T$ and $\boldsymbol{m}_z = [0, \ldots, M_z - 1]^T$. ⊗ denotes tensor product.

We assume that a signal with the OAM mode l is transmitting from the n_T-th antenna of U_T to the m-th ($m = 1, 2, \cdots, M$) passive reflecting element and from the m-th passive reflecting element to the n_R-th antenna of U_R. The free-space LoS channels from the n_T-th antenna of U_T to the m-th passive reflecting element is as follows [15][16][17]:

$$h_{n_T,m} = \frac{\beta\lambda}{4\pi d_{n_T,m}} exp\left(-j\frac{2\pi d_{n_T,m}}{\lambda}\right) \quad (5)$$

where β, λ, and $d_{n_T,m}$ are the antenna gain, wavelength of the carrier signal, and the distance between the n_T-th antenna of U_T and the m-th passive reflecting element.

$$d_{n_T,m} = \left\|\boldsymbol{\omega}_{I,m} - \boldsymbol{\omega}_{T,n_T}\right\| \quad (6)$$

where $\omega_{I,m}$ denotes the m-th column of Ω_I. $\boldsymbol{H_{T,I}} \in \mathbb{C}^{M\times N_T}$ is the LOS channel matrix between U_T and the passive reflecting element of the IRS. Similarly, the free-space LoS channels from the n_T-th antenna of U_T to the m-th passive reflecting element is as follows:

$$h_{m,n_R} = \frac{\beta\lambda}{4\pi d_{m,n_R}} exp\left(-j\frac{2\pi d_{m,n_R}}{\lambda}\right) \tag{7}$$

where $\beta, \lambda, d_{n_T,m}$ are the antenna gain, wavelength of the carrier signal, the distance between the m-th passive reflecting element and the n_R-th antenna of U_R.

$$d_{m,n_R} = \|\boldsymbol{\omega}_{R,n_R} - \boldsymbol{\omega}_{I,m}\| \tag{8}$$

$\boldsymbol{H_{I,R}} \in \mathbb{C}^{N_R \times M}$ is the LOS channel matrix between U_R and the passive reflecting element of the IRS.

At U_T, the transmit signal vector $\boldsymbol{s} \in \mathbb{C}^N$ is expressed as [16]

$$\boldsymbol{s} = \boldsymbol{F}^H \boldsymbol{Px} \tag{9a}$$

$$\boldsymbol{F}^H_{n_T,l} = \frac{1}{\sqrt{N_T}} \exp(jl\varphi_{T,n_T}) \tag{9b}$$

where $\boldsymbol{x} \in \mathbb{C}^L$ is the modulated signal vector, $\boldsymbol{F^H} \in \mathbb{C}^{N_T \times L}$ is the inverse discrete Fourier transform (IDFT) matrix of U_T, and $\boldsymbol{P} = diag(\sqrt{p_0},\ldots,\sqrt{p_{L-1}}) \in \mathbb{C}^{L\times L}$ denotes the power allocation matrix.

At the IRS, the received signal vector $\boldsymbol{r} \in \mathbb{C}^M$ is represented by

$$\boldsymbol{r} = \boldsymbol{H_{T,I}F^H Px} \tag{10}$$

At U_R, the received signal vector $\boldsymbol{y} \in \mathbb{C}^L$ is represented by

$$\widehat{\boldsymbol{y}} = \boldsymbol{F}(\boldsymbol{H_{I,R}\Theta r} + \boldsymbol{n}) = \boldsymbol{FH_{I,R}\Theta H_{T,I}F^H Px} + \boldsymbol{Fn} \tag{11a}$$

$$\boldsymbol{F}_{l,n_R} = \frac{1}{\sqrt{N_T}} \exp(jl\,\varphi_{R,n_R}) \tag{11b}$$

where $\boldsymbol{F} \in \mathbb{C}^{L\times N_R}$ is the discrete Fourier transform (DFT) matrix of U_R. $\boldsymbol{n} \in \mathbb{C}^{N_R}$ is the Gaussian noise vector with variance σ^2. For simplicity, we assume that there is no signal coupling in the reflection by neighboring IRS elements, i.e., all IRS elements reflect the incident signals independently. Moreover, $\boldsymbol{\Theta} = diag(\boldsymbol{\theta}^H) \in \mathbb{C}^{M\times M}$ denotes the diagonal phase shift vector of the IRS with $\boldsymbol{\theta} = [\theta_1, \cdots, \theta_m, \cdots, \theta_M]^T, |\theta_m| = 1$.

B. System Capacity Analysis

IMI cancellation method, equalization is conducted to eliminate IMI from all OAM modes [6], [7], [19]. Using linear filtering as an equalization technique, the received signal vector after equalization $\widehat{\boldsymbol{x}} \in \mathbb{C}^L$ is given by

$$\widehat{\boldsymbol{x}} = \boldsymbol{W}\widehat{\boldsymbol{y}} = \boldsymbol{W}(\boldsymbol{\Sigma x} + \boldsymbol{Fn}) \tag{12a}$$

$$\boldsymbol{\Sigma} = \boldsymbol{FH_{I,R}}\Theta\boldsymbol{H_{T,I}F^H P} \tag{12b}$$

where $\boldsymbol{\Sigma}$ are the equalization filter coefficient. Using the linear filtering based on minimum mean square error (MMSE) as the equalization criterion [20], the weighting matrix of MMSE $\boldsymbol{W} \in \mathbb{C}^{L\times L}$ is given as

$$\boldsymbol{W} = \left(\boldsymbol{\Sigma^H\Sigma} + \frac{P_n}{P_x}\boldsymbol{I_L}\right)^{-\boldsymbol{1}} \boldsymbol{\Sigma^H} \tag{13}$$

where P_x, P_n, $\boldsymbol{I_L}$ are the transmit power, noise power, and the identity matrix, respectively.

The received signal of the l-th OAM mode after equalization $\widehat{\boldsymbol{x}}_l$ is calculated as the desired signal component, IMI component, and noise component, respectively [21][22]. The powers of these components are calculated as follows:

$$\boldsymbol{\gamma}_l = \frac{|u_{l,l}|^2 p_l}{\sum_{k\neq l}|u_{l,k}|^2 p_k + \sum_{l\in\mathcal{L}}|\boldsymbol{w_{l,i}F}_{l,n_R}|^2\sigma^2} \tag{14a}$$

$$\boldsymbol{U} = \boldsymbol{WFH_{I,R}\Theta H_{T,I}F^H} \tag{14b}$$

where $u_{l,k}$ is the element of the l-th row and the k-th column of $\boldsymbol{U} \in \mathbb{C}^{L\times L}$, $\boldsymbol{\gamma}_l \in \mathbb{C}^L$ is SINR of the l-th OAM mode when considering noise and interference from other OAM modes, and $\boldsymbol{w_{l,i}}$ is the i-th row vector of $\boldsymbol{W}$. The system capacity $\boldsymbol{C}$ of UCA-based OAM communication is calculated as

$$\boldsymbol{C} = \sum_{l\in\mathcal{L}} \log_2(1 + \boldsymbol{\gamma}_l) \tag{15}$$

III. Communication Model

To maximize the system capacity of all OAM modes by optimizing the transmission power allocation [23] and the IRS's phase shift under the max transmission power budget of U_T and unit-modulus constraints of the IRS's reflecting phase shifts.

A. Optimizing the Transmit Power Allocation Algorithm

To maximize the system of all OAM modes, the problem of optimizing $\boldsymbol{p}$ can be formulated as

$$\max_{\boldsymbol{p}\geq\boldsymbol{0}} \sum_{l\in\mathcal{L}} \log(1 + \boldsymbol{\gamma}_l) \tag{16}$$

With fixed $\boldsymbol{\theta}$, the optimization problem (16) can be reformulated as

$$\max_{\boldsymbol{p}\geq\boldsymbol{0}} \sum_{l\in\mathcal{L}} \log(1 + \boldsymbol{u}_l^T\boldsymbol{p}) - \log(1 + \boldsymbol{u}_{-l}^T\boldsymbol{p}) \tag{17a}$$

$$s.t.\, \boldsymbol{p^T 1_L} \leq P_{max} \tag{17b}$$

where $\boldsymbol{u}_l = \left[|u_{l,0}|^2, \cdots, |u_{l,L-1}|^2\right]$,

$\boldsymbol{u}_{-l} = \left[|u_{l,0}|^2, \cdots, |u_{l,l-1}|^2, 0, |u_{l,l+1}|^2, \cdots, |u_{l,L-1}|^2\right]$.

In [8], the majorization-minimization (MM)-based approach is proposed to solve the surrogate function for non-convex function (17a). The surrogate function for (17a) can be expressed as the following lemma:

Lemma 1: In the (t + 1)-th iteration, a valid surrogate function for $f_l(\boldsymbol{p}) = \log(1 + \boldsymbol{u}_l^T\boldsymbol{p}) - \log(1 + \boldsymbol{u}_{-l}^T\boldsymbol{p})$ is

$$\bar{f}_l(\boldsymbol{p}; \boldsymbol{p}^{(t)}) \triangleq -\xi_l p^T p + b_l^T p + c_l \tag{18}$$

where

$$\xi_l = \frac{1}{2}\lambda_{max}(\boldsymbol{u}_l\boldsymbol{u}_l^T), b_l = \bar{b}_l - \tilde{b}_l, c_l = \bar{c}_l - \tilde{c}_l \tag{19a}$$

$$\bar{b}_l = \frac{\boldsymbol{u}_l}{1 + \boldsymbol{u}_l^T p^{(t)}} + 2\xi_l p^{(t)}, \tilde{b}_l = \frac{\boldsymbol{u}_{-l}}{1 + \boldsymbol{u}_{-l}^T p^{(t)}} \tag{19b}$$

$$\bar{c}_l = \log(1 + \boldsymbol{u}_l^T\boldsymbol{p}) + \xi_l\|p^{(t)}\|^2 - \bar{b}_l^T p^{(t)} \tag{19c}$$

$$\tilde{c}_l = \log(1 + \boldsymbol{u}_{-l}^T\boldsymbol{p}) - \tilde{b}_l^T p^{(t)} \tag{19d}$$

$\lambda_{max}(\boldsymbol{A})$ denotes the maximum eigenvalue of $\boldsymbol{A}$.

Here, we propose the ℓ_2-ball projection method [24] instead of the ℓ_1-ball projection method to drive a closed-form solution. The ℓ_2-ball projection method tend to be more accurate in the prediction accuracy than the ℓ_1-ball projection method [25] because the transmission power can be assigned to all OAM modes.

In [10], in the $(t+1)$-th iteration, the interior point method is proposed to re-express the optimization problem to the following convex projection problem.

$$\min_{\boldsymbol{p}\geq\boldsymbol{0}} \|\boldsymbol{p}-\boldsymbol{q}\| \tag{20a}$$

$$\boldsymbol{p}^{\boldsymbol{T}}\boldsymbol{1}_L \leq P_{max} \tag{20b}$$

where

$$\boldsymbol{q} = \frac{\sum_{l\in\mathcal{L}} b_l}{2\sum_{l\in\mathcal{L}} \xi_l} = [q_0, \cdots, q_{L-1}]^T \tag{21}$$

The closed-form solution based on ℓ_2-ball projection method can be obtained as

$$p_l^* = \begin{cases} q_l & \text{if} \sum_{l\in\mathcal{L}} q_l \leq P_{max} \\ \dfrac{q_l}{1+\beta} & \text{if} \sum_{l\in\mathcal{L}} q_l > P_{max} \end{cases} \tag{22}$$

$$\beta = \frac{1}{\gamma+1}\left(\sum_{i=0}^{\gamma}[\varphi]^+ - P_{max}\right) \tag{23}$$

$$\gamma = \max_{l\in\mathcal{L}}\left\{l \middle| [\varphi]^+ - \frac{1}{l+1}\left(\sum_{k=0}^{l}[\varphi_k]^+ - P_{max}\right) > 0\right\} \tag{24}$$

where $[a]^+$ denotes $max\{a, 0\}$, and $\boldsymbol{\varphi} = [\varphi_0, \ldots, \varphi_{L-1}]^T$ denotes the vector obtained via sorting $\boldsymbol{q}$ in a descending order.

The whole algorithm for solving (14) is summarized in Algorithm 1.

Algorithm 1: Optimizing the transmission power allocation algorithm.

1: Initialize: $t := 0, \boldsymbol{p}^{(0)}$;
2: Repeat: Calculate $\{b_l\}$ and $\{\xi_l\}$ in $\mathbf{q}$ with $\boldsymbol{p}^{(t)}$ according to (19a) and (19b);
Sort q in a descending order; Update $\boldsymbol{p}^{(t+1)}$ according to (22);
$t := t+1$;
3: Until: $\left|\boldsymbol{p}^{(t+1)} - \boldsymbol{p}^{(t)}\right| < \epsilon_p$

B. Optimizing the IRS's Reflecting Phase Shift

To maximize the system capacity of all OAM modes, the problem of optimizing $\boldsymbol{\theta}$ can be formulated as

$$\max_{\theta} \sum_{l\in\mathcal{L}} \log_2\left(1 + \frac{p_l\left|\boldsymbol{\theta}^H \overline{w}_{l,l}\right|^2}{\sum_{k\neq l} p_k \left|\boldsymbol{\theta}^H \overline{w}_{l,k}\right|^2}\right) \tag{25}$$

where

$$\overline{\boldsymbol{w}}_{l,k} = \frac{1}{\sqrt{N_R N_T}} diag(\boldsymbol{F}_l \boldsymbol{H}_{I,R})\boldsymbol{H}_{T,I}\boldsymbol{F}_l^H, k, l \in \mathcal{L} \tag{26a}$$

$$\boldsymbol{F}_l^H = \frac{1}{\sqrt{N_T}}\left[\exp(jl\varphi_{T,0}), \cdots, \exp(jl\varphi_{R,N_T})\right]^T \in \mathbb{C}^{N_T} \tag{26b}$$

$$\boldsymbol{F}_l = \frac{1}{\sqrt{N_R}}\left[\exp(jl\varphi_{R,0}), \cdots, \exp(jl\varphi_{R,N_R})\right] \in \mathbb{C}^{N_R} \tag{26c}$$

In [10], a iterative weighted MMSE approach is proposed to find the optimal $\boldsymbol{\theta}$ in (23). The whole algorithm for solving (25) is expressed in Algorithm 2.

Algorithm 2: Optimizing the IRS's reflecting phase shift Algorithm.

1: Initialize: $t := 0, \boldsymbol{\theta}^{(0)}$;
2: Repeat: Update $\lambda^{(t+1)}$ according to (27) with $\boldsymbol{\theta}^{(t)}$;
Update $\mu^{(t+1)}$ according to (28) with $\boldsymbol{\theta}^{(t)}$;
Update $\boldsymbol{\theta}^{(t+1)}$ according to (31) and (32) with $\lambda^{(t+1)}$ and $\mu^{(t+1)}$;
$t := t+1$
3: Until: $\left|\boldsymbol{\theta}^{(t+1)} - \boldsymbol{\theta}^{(t)}\right| < \epsilon$

where

$$\lambda_l = \frac{\sqrt{p_l}\boldsymbol{\theta}^H \overline{w}_{l,l}}{\sum_{k\in\mathcal{L}} p_k \left|\boldsymbol{\theta}^H \overline{w}_{l,k}\right|^2 + \sigma^2} \tag{27}$$

with fixed θ and μ,

$$\mu_l = 1 + \frac{p_l\left|\boldsymbol{\theta}^H \overline{w}_{l,l}\right|^2}{\sum_{k\in\mathcal{L}} p_k \left|\boldsymbol{\theta}^H \overline{w}_{l,k}\right|^2 + \sigma^2} \tag{28}$$

with fixed θ and λ,

$$\boldsymbol{R} = \sum_{\boldsymbol{l}\in\mathcal{L}}\left[\mu_l|\lambda_l|^2 \sum_{\boldsymbol{k}\in\mathcal{L}} p_k \overline{w}_{l,k}\overline{w}_{l,k}^H\right] \tag{29}$$

with fixed μ and λ,

$$\boldsymbol{r} = -\boldsymbol{2}\sum_{l\in\boldsymbol{\mathcal{L}}} \mu_l \sqrt{p_l}\lambda_l^H \overline{w}_{l,k}^H \in \mathbb{C}^M \tag{30}$$

$$\widehat{\boldsymbol{R}} = \begin{bmatrix} \boldsymbol{R} & \dfrac{1}{2}\boldsymbol{r} \\ \dfrac{1}{2}\boldsymbol{r}^{\boldsymbol{H}} & 0 \end{bmatrix} \in \mathbb{C}^{(M+1)\times(M+1)} \tag{31}$$

$$\widetilde{\boldsymbol{R}} = -\widehat{\boldsymbol{R}} + \boldsymbol{\lambda}_{\boldsymbol{max}}(\widehat{\boldsymbol{R}})\boldsymbol{I}$$

The optimal solution of $\widehat{\boldsymbol{\theta}}$ can be obtained via the fixed-point iteration, then in the t-th iteration, $\widehat{\boldsymbol{\theta}}$ can be updated as

$$\widehat{\boldsymbol{\theta}}^{(t)} = \exp\left(j\arg\left(\widetilde{\boldsymbol{R}}\widehat{\boldsymbol{\theta}}^{(t-1)}\right)\right) \tag{32}$$

Finally, after convergence, the solution to problem (32) can be recovered by

$$\boldsymbol{\theta}^* = \frac{\left[\widehat{\theta}_{\boldsymbol{1}}^{(t)}, \cdots, \widehat{\theta}_{\boldsymbol{M}}^{(t)}\right]^{\boldsymbol{T}}}{\widehat{\theta}_{\boldsymbol{M+1}}^{(t)}} \tag{33}$$

C. Optimizing the system capacity of all OAM modes

The whole alternating algorithm for optimizing $\boldsymbol{p}$ and $\boldsymbol{\theta}$ in (16) and (25) can be expressed in Algorithm 3.

Algorithm 3: Optimizing the transmit power allocation and the IRS's reflecting phase shift algorithm.

1: Initialize: $t := 0, \boldsymbol{p}^{(0)}, \boldsymbol{\theta}^{(0)}$;
2: Repeat: Update $\boldsymbol{p}^{(t+1)}$ via Algorithm 1 with $\boldsymbol{p}^{(t)}$ and $\boldsymbol{\theta}^{(t)}$;
Update $\boldsymbol{\theta}^{(t+1)}$ via Algorithm 2 with $\boldsymbol{p}^{(t+1)}$ and $\boldsymbol{\theta}^{(t)}$;
$t := t+1$;
3: Until: $\left|\boldsymbol{p}^{(t+1)} - \boldsymbol{p}^{(t)}\right| < \epsilon$ and $\left|\boldsymbol{\theta}^{(t+1)} - \boldsymbol{\theta}^{(t)}\right| < \epsilon_\theta$

TABLE 1. SYSTEM PARAMETERS

Carrier frequency f_c	10 GHz
The number of antenna elements N	8
The number of multiplexed OAM modes L	$5\ (0, \pm 1, \pm 2)$
Radius of U_T, U_R	0.6 m
Antenna gain β^2	15 dB
$x_{I,O}$	1 m
P_{max}/σ^2	50 dB
The max transmission power budget P_{max}	5 W
The number of passive reflecting elements at the IRS M	256
Absolute tolerance ϵ_p	5×10^{-3}
Absolute tolerance ϵ_θ	256×10^{-3}
The distance between U_T and U_R	40 m
d_y, d_z	0.06 m

IV. SIMULATION RESULTS

In this section, we present the effectiveness of the IMI cancellation method by comparing it with the IMI cancellation method from all OAM modes in terms of the SINR and system capacity. We also present the ℓ_2-ball projection method by comparing it with the ℓ_1-ball projection method. Table 1 shows the system parameters of the system model.

In Fig. 2, the legend is as follows. “IMI cancellation + L2-ball” denotes applying the ℓ_2-ball projection method to optimizing power allocation and applying IMI cancellation. “IMI cancellation + L1-ball” denotes applying the ℓ_1-ball projection method and applying IMI cancellation. “L2-ball” denotes applying the ℓ_2-ball projection method with no IMI cancellation. “L1-ball” denotes applying the ℓ_1-ball projection method with no IMI cancellation.

From Fig. 2, it is observed that system capacity increase applying IMI cancellation effectively both of the ℓ_1-ball projection method and the ℓ_2-ball projection method. It is also observed that the maximum system capacity can be achieved effectively by applying the ℓ_2-ball projection method than the ℓ_1-ball projection method when the IRS is placed in the middle.

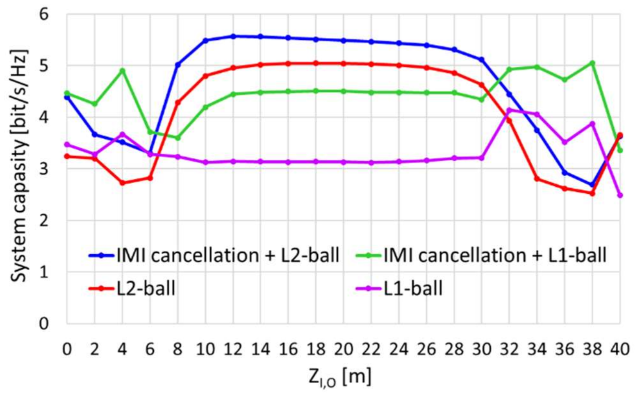

Figure 2. The system capacity of some different schemes versus the distance between U_T and the IRS along the z-axis, $z_{I,O}$

This is because the longer distance between U_T and the IRS or the IRS and U_R constrain the system capacity owing to the deteriorated divergence effect as (7) shows. Those results indicate that system capacity increase applying the IMI cancellation method. Those result also indicate that system capacity increase applying the ℓ_2-ball projection method when the IRS is located closer to the middle.

V. CONCLUSIONS

In this paper, the IMI cancellation method and the ℓ_2-ball projection method optimize the transmit power allocation for OAM modes in IRS-assisted OAM communication systems. The IMI cancellation method is shown to achieve increasing the maximum system capacity. The ℓ_2-ball projection method is shown to achieve increasing the maximum system capacity as compared to the ℓ_1-ball projection method, but it is limited to when the IRS is placed near the middle. Simulation results indicate that the IMI cancellation method and the ℓ_2-ball projection method can be applied to IRS-assisted OAM-based communication systems and increase the system capacity of the NLoS OAM-MIMO communication system. In the future, we are going to discuss the switching between the ℓ_1-ball projection method and the ℓ_2-ball projection method depending on the transmission system. We are also going to discuss the optimal placement of IRS according to the surrounding multipath environment using the ray tracing method.

REFERENCES

[1] ITU, “M.2083: IMT Vision - "Framework and overall objectives of the future development of IMT for 2020 and beyond”, Recommendation M.2083, Sep. 2015.

[2] L. Allen, M. W. Beijersbergen, R. J. C. Spreeuw and J. P. Woerdman, "Orbital angular momentum of light and the transformation of Laguerre-Gaussian laser modes", Phys. Rev. A, vol. 45, no. 11, pp. 8185-8189, June. 1992.

[3] Y. Ren, L. Li, G. Xie, Y. Yan, Y. Cao, H. Huang, N. Ahmed, Z. Zhao, P. Liao, C. Zhang, G. Caire, A. F. Molisch, M. Tur, and A. E. Willner, “Line-of-sight millimeter-wave communications using orbital angular momentum multiplexing combined with conventional spatial multiplexing,” IEEE Trans. Wireless Commun. vol. 16, no. 5, pp. 3151–3161, May 2017.

[4] Y. Yuan, Z. Zhang, J. Cang, H. Wu and C. Zhong, "Capacity analysis of UCA-based OAM multiplexing communication system," 2015 International Conference on Wireless Communications & Signal Processing (WCSP), 2015, pp. 1-5.

[5] H. Sasaki, Y. Yagi, T. Yamada, and D. Lee, “Field Experimental Demonstration on OAM-MIMO Wireless Transmission on 28 GHz Band”, 2019 IEEE Globecom Workshops.

[6] R. Chen, H. Xu, J. Li, and Y. Zang, “Misalignment-robust receiving scheme for UCA-based OAM communication systems,” Proc. IEEE 85th Veh. Technol. Conf. (VTC 2017-Spring), pp. 1–5, June 2017.

[7] R. Chen, W.-X. Long, X. Wang, and L. Jiandong, “Multi-mode OAM radio waves: Generation, angle of arrival estimation and reception with UCAs,” IEEE Trans. Wireless Commun., vol. 19, no. 10, pp. 6932–6947, Oct. 2020.

[8] W. Jie, Y. Wang, T. Hu, J. Liu, D. Yang and Q. Chen, "Two-ray multipath propagation of MIMO-based OAM radio communications," 2019 International Symposium on Antennas and Propagation (ISAP), 2019, pp. 1-3.

[9] M. Jian, "NLOS OAM-MIMO Transmission: Misaligned Channel Analysis and Pre-processing Scheme Design," 2020 International

Wireless Communications and Mobile Computing (IWCMC), 2020, pp. 1866-1871, doi: 10.1109/IWCMC48107.2020.9148466.

[10] Y. Li, M. Jiang, G. Zhang and M. Cui, "Achievable Rate Maximization for Intelligent Reflecting Surface-Assisted Orbital Angular Momentum-Based Communication Systems," in IEEE Transactions on Vehicular Technology, vol. 70, no. 7, pp. 7277-7282, July 2021.

[11] Q. Wu, S. Zhang, B. Zheng, C. You and R. Zhang, "Intelligent Reflecting Surface-Aided Wireless Communications: A Tutorial," in IEEE Transactions on Communications, vol. 69, no. 5, pp. 3313-3351, May 2021.

[12] B. Zheng, C. You and R. Zhang, "Fast Channel Estimation for IRS-Assisted OFDM," in IEEE Wireless Communications Letters, vol. 10, no. 3, pp. 580-584, March 2021.

[13] B. Thid, H. Then, J. Sjholm, K. Palmer, J. E. S. Bergman, T. D. Carozzi, et al., "Utlilization of photon orbital angular momentum in the low-frequency radio domain", Phys. Rev. Lett., vol. 99, no. 8, pp. 087701, Aug. 2007.

[14] Yingjie Zhang, W. Feng and N. Ge, "On the restriction of utilizing orbital angular momentum in radio communications," 2013 8th International Conference on Communications and Networking in China (CHINACOM), 2013, pp. 271-275.

[15] H. Tian, "Beam axis detection and alignment for uniform circular array-based orbital angular momentum wireless communication," IET Journals, ISSN 1751-8628, 2015.

[16] L. Liang, W. Cheng, W. Zhang and H. Zhang, "Orthogonal Frequency and Mode Division Multiplexing for Wireless Communications," 2018 IEEE Global Communications Conference (GLOBECOM), 2018, pp. 1-7.

[17] H. Jing, W. Cheng, X. Xia and H. Zhang, "Orbital-Angular-Momentum Versus MIMO: Orthogonality, Degree of Freedom, and Capacity," 2018 IEEE 29th Annual International Symposium on Personal, Indoor and Mobile Radio Communications (PIMRC), 2018, pp. 1-7

[18] L. Sung, D. Park and D. Cho, "Performance analysis of orbital angular momentum(OAM) transmission using dual polarization antenna based uniform circular array architecture," 2016 13th IEEE Annual Consumer Communications & Networking Conference (CCNC), 2016, pp. 517-522.

[19] S. Saito, H. Suganuma, K. Ogawa and F. Maehara, "Performance Enhancement of OAM-MIMO Using Successive Interference Cancellation," 2019 IEEE 89th Vehicular Technology Conference (VTC2019-Spring), 2019, pp. 1-5.

[20] K. A. Opare, Y. Kuang, J. J. Kponyo, K. S. Nwizege and P. I. Tebe, "The Effect of Receiver-Side Circular Antenna Arrays on Bit Error Probability in a Wireless Line-of-Sight OAM Communication System," 2015 Fifth International Conference on Advanced Computing & Communication Technologies, 2015, pp. 614-620.

[21] H. Jing, W. Cheng, Z. Li and H. Zhang, "Concentric UCAs based low-order radio vortex wireless communications with co-mode interference," 2017 IEEE/CIC International Conference on Communications in China (ICCC), 2017, pp. 1-6.

[22] W. Cheng, H. Jing, W. Zhang, Z. Li and H. Zhang, "Achieving Practical OAM Based Wireless Communications with Misaligned Transceiver," ICC 2019 - 2019 IEEE International Conference on Communications (ICC), 2019, pp. 1-6.

[23] M. Qu, Y. Wang, X. Liao, S. Liao and J. Zhou, "Optimal Power Allocation Algorithm for Multi-Mode OFDM-OAM Communication Systems in Multipath Channel," in IEEE Access, vol. 8, pp. 204342-204351, 2020.

[24] Crammer, K., Dekel, O., Keshet, J., Shalev-Shwartz, S., and Singer, Y. (2006). Online passive aggressive algorithms.

[25] J. Duchi, S. Shalev-Shwartz, Y. Singer, and T. Chandra, "Efficient projections onto the ℓ_1-ball for learning in high dimensions," in Proc. Int. Conf. Mach. Learn., Helsinki, Finland, 2008, pp. 272–279.

Kosei Ono (M'20) received the B.E. degree in Communications and Computer Engineering from Waseda University, Japan, in 2020. He is currently pursuing the M.S. degree with the department of Computer Science and Communications Engineering, School of Fundamental Science and Engineering, Waseda University, Japan. His research interests include OAM and energy harvesting system design.

Kazutoshi Yoshii (M'19) received the B.E. degree in Communications and Computer Engineering from Waseda University, Japan, in 2018, and the M.E. degree in Computer Science and Communications Engineering from Waseda University, Japan, in 2020, respectively. He is currently the Research Associate with the department of Computer Science and Communications Engineering, School of Fundamental Science and Engineering, Waseda University, Japan. His research interests include HF communication and ionospheric propagation.

Megumi Saito (M'15) received M.S. degree from Graduate School of Global Information and Telecommunication Studies, Waseda University, Japan in 2014. She is a Ph.D. candidate at Department of Computer Science and Communications Engineering, School of Fundamental Science and Engineering. She is also a research associate Waseda University, Japan. Her research interest includes D2D, Cooperative Access scheme in Cellular Networks.

Zhenni Pan (M'11, SM'13) received the B.S. degree in computer science engineering from China Agricultural University, Beijing, China, in 2007. She received the M.S. and Ph.D. degree in information and telecommunications from the Graduate School of Global Information and Telecommunication Studies (GITS), Waseda University, Japan, in 2011 and 2018, respectively. She was a research associate from 2013 to 2018 at Waseda University. Currently, she is an assistant professor at Global Center for Science and Engineering, Faculty of Science and Engineering, Waseda University. Her research interests include green wireless communications, mobile communications, MIMO systems, wireless sensor networks, UAV and optical communication.

Jiang Liu (M'05, SM'09, F'18) received the B.E. degree in electronics engineering from Chong Qing University of Technology, China, in 2001, and the M.S. and Ph.D. degree in information and telecommunications from the Graduate School of Global Information and Telecommunication Studies (GITS), Waseda University, Japan, in 2006 and 2012 respectively. She was a research associate from 2009 to 2012, and an assistant professor from 2013 to 2017 at Waseda University. Currently, she is an associate professor at Faculty of Science and Engineering, Waseda University. Her main fields of research interests include optical wireless communication, cellular system design, sensor network, and smart grid systems.

Shigeru Shimamoto (M'94) received the B.E. and M.E. degrees from the University of Electro-Communications, Tokyo, Japan, in 1985 and 1987, respectively. He received the Ph.D. degree from Tohoku University, Sendai, Japan, in 1992. He joined NEC Corporation from 1987 to 1991. From 1991 to 1992, he was a research associate in the University of Electro-Communications, Tokyo, Japan. He was a research associate in Gunma University, Gunma, Japan, from 1992 to 1993. From 1994 to 2000, he was an associate professor in the Graduate School of Global Information and Telecommunication Studies (GITS), Waseda University, Tokyo, Japan. Since 2001, he has been a professor in the Graduate School of GITS, Waseda University. He was a visiting professor of E.E. at Stanford University in 2008. His main fields of research interests include satellite communications, mobile communications, optical wireless communications, ad-hoc networks, sensor networks, and body area networks.